blood®
Regular Article

RED CELLS, IRON, AND ERYTHROPOIESIS

p53 activation during ribosome biogenesis regulates normal erythroid differentiation

Salomé Le Goff,[1,2,*] Ismael Boussaid,[1,*] Celia Floquet,[1,†] Anna Raimbault,[1,†] Isabelle Hatin,[3] Charlotte Andrieu-Soler,[2,4] Mohammad Salma,[4] Marjorie Leduc,[1,5] Emilie-Fleur Gautier,[1,2,5] Boris Guyot,[6] Diane d'Allard,[1] Nathalie Montel-Lehry,[7] Sarah Ducamp,[1,2] Amandine Houvert,[1] François Guillonneau,[1,5] Stéphane Giraudier,[8] Elisabeth Cramer-Bordé,[1] François Morlé,[9] Jean-Jacques Diaz,[10] Olivier Hermine,[2,11] Naomi Taylor,[2,4] Sandrina Kinet,[2,4] Frédérique Verdier,[1,2] Rose-Ann Padua,[8] Narla Mohandas,[12] Pierre-Emmanuel Gleizes,[7] Eric Soler,[2,4] Patrick Mayeux,[1,2,5] and Michaela Fontenay[1,2,13]

[1]Université de Paris, Institut Cochin, Unité Mixte de Recherche (UMR) 8104, Centre National de la Recherche Scientifique (CNRS), INSERM U1016, Paris, France; [2]Université de Paris, Laboratoire d'Excellence (LabEx) du Globule Gouge (GR-Ex), Paris, France; [3]Institute for Integrative Biology of the Cell (I2BC), Commissariat à l'Énergie Atomique et aux Énergies Alternatives (CEA), CNRS, Université Paris-Sud, Université Paris-Saclay, Gif-sur-Yvette, France; [4]Institut de Génétique Moléculaire Montpellier (IGMM), Université de Montpellier, CNRS, Montpellier, France; [5]Université de Paris, Plateforme de Protéomique 3P5, Paris, France; [6]Department Signaling of Tumor Escape, Centre de Recherche en Cancérologie de Lyon, Université Claude Bernard Lyon 1, UMR 5286, CNRS, INSERM U1052, Lyon, France; [7]Laboratoire de Biologie Moléculaire Eucaryote, Centre de Biologie Intégrative (CBI), CNRS, Université Paul Sabatier, Université de Toulouse, Toulouse, France; [8]Université de Paris, Institut de Recherche Saint Louis, UMR-S1131, Paris, France; [9]Institut NeuroMyoGène (INMG), UMR 5310, Université Claude Bernard Lyon 1, CNRS, INSERM U1217, Villeurbanne, France; [10]Centre Léon Bérard, Centre de Recherche en Cancérologie de Lyon, Université Lyon, Université Claude Bernard Lyon 1, CNRS 5286, INSERM 1052, Lyon, France; [11]Imagine Institute, Université de Paris, INSERM U1163, Paris, France; [12]Red Cell Physiology Laboratory, New York Blood Center, New York, NY; and [13]Service d'Hématologie Biologique, Hôpital Cochin, Assistance Publique–Hôpitaux de Paris, Centre-Université de Paris, Paris, France

KEY POINTS

- **Ribosome biogenesis arrests at the transition between early and late basophilic erythroblasts.**
- **p53 is activated in immature erythroid precursors and drives an erythroid transcriptional program, implying an interplay with GATA1.**

The role of ribosome biogenesis in erythroid development is supported by the recognition of erythroid defects in ribosomopathies in both Diamond-Blackfan anemia and 5q− syndrome. Whether ribosome biogenesis exerts a regulatory function on normal erythroid development is still unknown. In the present study, a detailed characterization of ribosome biogenesis dynamics during human and murine erythropoiesis showed that ribosome biogenesis is abruptly interrupted by the decline in ribosomal DNA transcription and the collapse of ribosomal protein neosynthesis. Its premature arrest by the RNA Pol I inhibitor CX-5461 targeted the proliferation of immature erythroblasts. p53 was activated spontaneously or in response to CX-5461, concomitant to ribosome biogenesis arrest, and drove a transcriptional program in which genes involved in cell cycle–arrested, negative regulation of apoptosis, and DNA damage response were upregulated. RNA Pol I transcriptional stress resulted in nucleolar disruption and activation of the ATR-CHK1-p53 pathway. Our results imply that the timing of ribosome biogenesis extinction and p53 activation is crucial for erythroid development. In ribosomopathies in which ribosome availability is altered by unbalanced production of ribosomal proteins, the threshold downregulation of ribosome biogenesis could be prematurely reached and, together with pathological p53 activation, prevents a normal expansion of erythroid progenitors. (*Blood*. 2021;137(1):89-102)

Introduction

Erythropoiesis originates from the commitment of hematopoietic stem cells to erythroid progenitors. The terminal differentiation starts with the appearance of immature proerythroblasts (proEs) that divide to give rise, first to early basophilic erythroblasts (baso1), then to late basophilic erythroblasts (baso2). The next 2 cell divisions produce mature polychromatic (polyE) and orthochromatic (orthoE) erythroblasts with reduction in cell size and changes in cell surface marker expression.[1-3] The transition between proliferation and differentiation depends on the evolutionary capacities of cells to respond to cytokines. Stem cell factor (SCF) sustains renewal of progenitors and immature precursors, whereas the extinction of the SCF receptor c-Kit from basoEs is necessary for differentiation after erythropoietin (EPO) exposure. Morphological changes are mediated by transcriptome reprogramming,[4-6] mainly involving activation or repression of GATA1 target genes.[7,8] At the translation regulation level, the cellular ribosome concentration mediates the effects of messenger RNA (mRNA) amount and rate of translation initiation on protein synthesis.[9] Ribosome content depends on the rate of ribosome biogenesis, which starts in the nucleolus with the transcription of ribosomal DNA (rDNA) into a 45S ribosomal RNA

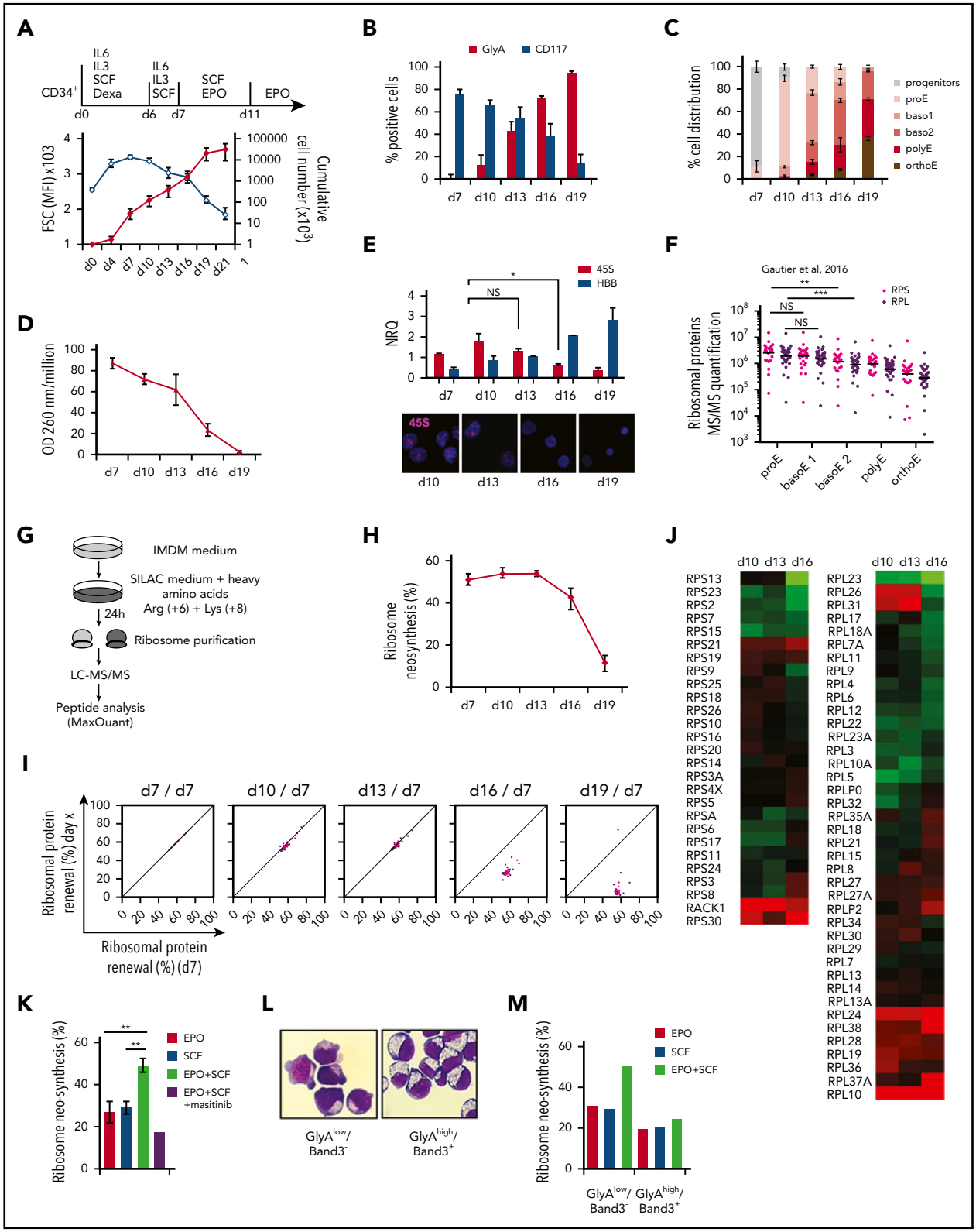

Figure 1. Kinetics of ribosome neosynthesis during erythroid differentiation. Human primary erythroblasts were derived from CD34$^+$ progenitors cultured for 6 days in the presence of SCF, IL-6, IL-3, and dexamethasone (1 μM); with SCF, IL-6, and IL-3 for 1 day; with SCF and EPO between days 7 and 11; and then with EPO alone. (A) Amplification curve and cell size. Human erythroblast proliferation was expressed as the cumulative number of cells at each indicated time (closed symbols). Cell size was measured using forward scatter (FSC) light expressed as the mean fluorescence intensity (MFI; open symbols). Means ± SEM of 4 experiments. (B) Expression of the SCF receptor CD117 and GlyA by flow cytometry during human erythroblast differentiation. (C) Proportion of progenitor, ProE, baso1, baso2, polyE, and orthoE cells at the indicated days, determined by May-Grünwald-Giemsa–stained cytospins. Mean ± SEM of 4 independent experiments. (D) *RNA* quantification in ribosome fractions. Quantities of RNA in ribosomes of human erythroblasts purified by ultracentrifugation on sucrose gradient were measured at OD 260 nm per 10^6 cells. Mean ± SEM of 6 experiments. (E) Quantification (top) of pre-rRNA 45S and β-globin (HBB) transcripts by qRT-PCR. Transcripts amounts were normalized to *B2M* and *UBC* transcript amounts, and normalized relative quantities (NRQs)

(rRNA) precursor by RNA polymerase I (Pol I). This RNA precursor gradually assembles with ribosomal proteins (RPs) and is concomitantly cleaved into rRNAs, first in the nucleolus, then in the nucleoplasm and cytoplasm. This complex processing scheme leads to formation of the 40S subunit by 18S rRNA and small subunit RP (RPSs), whereas 28S and 5.8S rRNAs constitute the 60S subunit with 5S rRNA and large subunit RPs (RPLs).[10,11]

In pathological states that result in macrocytic anemia, such as congenital Diamond-Blackfan anemia or acquired 5q− syndrome, which are caused by point mutations or deletions in RP genes,[12-14] the ribosome pools in erythroid cells are diminished, suggesting that ribosome levels regulate differentiation.[15] Insufficient quantities of ribosomes account for a reduction of GATA1 mRNA translation initiation rate,[15-17] whereas the stress caused by impaired ribosome biogenesis induces stabilization and activation of p53 driving cell cycle arrest and apoptosis of erythroblasts.[18,19] Interestingly, the ribosome biogenesis machinery is the first downregulated cellular process when cells enter the final stages of erythroid maturation in human and mouse models.[16,20,21] Thus, ribosome biogenesis, per se, may have a regulatory role in normal erythroid differentiation by controlling pathways that remain to be defined.

In the present study, the collapse of ribosome neosynthesis in normal mature erythroblasts was concomitant with the activation of a p53-dependent transcriptional program, leading to cell cycle arrest.

Material and methods

Human and murine erythroblast cultures

Human CD34$^+$ progenitors were purified from cord blood units on MidiMacs system (Miltenyi Biotech, Bergisch Gladbach, Germany). Murine extensively self-renewing erythroblasts (ESREs) were derived from fetal livers. Cell differentiation was followed by cytological examination and by flow cytometry (supplemental Material, available on the *Blood* Web site).

qRT-PCR and microarrays

RNA was extracted with the QIAamp RNA Blood kit (Qiagen, Hilden, Germany). Quantitative reverse transcription-polymerase chain reaction (qRT-PCR) was performed with SYBR Green I Master Mix on a LC480 PCR system (Roche). Primer sequences are provided in supplemental Table 1. Gene expression data were generated with HTA 2.0 microarrays (Affymetrix, Santa Clara, CA) (supplemental Material).

Fluorescence in situ hybridization

Cells were fixed with 4% paraformaldehyde and permeabilized in 70% ethanol. Hybridization was performed at 37°C for ≥5 h in 10% formamide, 2.1× saline-sodium citrate, 0.5 μg/mL transfer RNA, 10% dextran sulfate, 250 μg/mL bovine serum albumin, 10 mM ribonucleoside vanadyl complexes, and 0.5 ng/μL 5′ETS probe conjugated to Alexa 647 (5′-AGACGAGAACGCCTGACA CGCACGGCAC-3′).[22] Images were obtained with a DMI6000 confocal fluorescence microscope (Leica, Wetzlar, Germany) and analyzed with ImageJ.

Ribosomal subunit profiling and rRNA quantification

Erythroblasts (10^7) were harvested and disrupted in 50 mM Tris-HCl (pH7.5) and 50 mM NaCl containing 1 mM dithiothreitol. Lysates were loaded onto 11.4 mL of 15% to 50% linear sucrose gradient and centrifuged at 39 000 rpm in a Beckman SW41Ti rotor at 4°C for 3 hours. Gradient analyses were performed at A_{260nm} with an absorbance detector (Teledyne ISCO, Lincoln, NE). RNA was quantified at optical density $(OD)_{260nm}$ on a 2100 Bioanalyzer (Agilent Scientific Instruments, Santa Clara, CA).

Stable isotope labeling by amino acids in cell culture and riboproteomics

Metabolic labeling was performed in Iscove's modified Dulbecco's medium (IMDM) minus L-lysine and L-arginine supplemented with 0.2 mg/mL $^{13}C_6$ L-arginine-HCl, 0.2 mg/mL $^{13}C_6$, $^{15}N_2$ L-lysine-2 HCl (Pierce, Rockford, IL), 80 μg/mL proline, and 15% serum substitute with bovine serum albumin insulin transferrin during 24 hours for human erythroblasts and 14 hours for murine ESREs. In some experiments, cells were preincubated with 50 nM CX-5461 for 24 hours before starting pulse and then processed for riboproteomics (supplemental Material).

Absolute quantification of ribosomal and erythroid-specific proteins

Label-free protein quantification was performed as described.[21] Mass spectrometry data were processed by MaxQuant, version 1.5.2.8, using human sequences from the Uniprot-Swiss-Prot database with a false-discovery rate below 1% for both peptides and proteins.[23] Results from MaxQuant were imported into Perseus software (version 1.5.1.6). The protein copy number per cell was then calculated with the Protein Ruler plugin of Perseus

Figure 1 (continued) were calculated. Mean NRQ ± SEM of 3 experiments. Fluorescence in situ hybridization (bottom) for pre-rRNA 45S in human erythroblasts at the indicated culture times. Slides were stained using a 5′ETS probe conjugated to Alexa 647. Images were obtained on a Leica DMI6000 inverted microscope with spinning disk and analyzed with ImageJ. *$P < .05$. (F) Absolute quantification of RPs by MS/MS plotted from publicly available data from Gautier et al.[20] Results are expressed as the median protein copy number of 4 independent experiments. **$P < .01$; ***$P < .001$, by Student *t* test. (G) Schematic experimental design of SILAC labeling. Human erythroblasts were metabolically labeled for 24 hours, and ribosomes were purified by differential centrifugation and analyzed by LC-MS/MS. IMDM, Iscove's modified Dulbecco's medium. (H) Kinetics of ribosome neosynthesis. In each experiment, the percentage of each neosynthesized RP was calculated as (H/H+L) ×100. Ribosome neosynthesis was defined as the median of neosynthesized RP percentages. Mean ± SEM of 4 experiments. (I) Concomitant decrease in RPL and RPS neosynthesis. The percentage of neosynthesis (calculated as in panel H) of each protein was plotted in 2-dimensional scatterplots to compare the value at each time point with the reference value at day 7. RPL: purple dots; RPS: pink dots. Results are representative of 4 independent experiments. (J) Comparison of the rate of neosynthesis of each RP at different time points of the human erythroid differentiation. The H/L ratio was normalized to the median of the H/L ratios of all RPs of the same subunit and transformed to log2 values. RPs in red are those with the highest rate of neosynthesis and incorporation into the ribosome. The heat maps are representative of 4 independent experiments. (K) Ribosome neosynthesis by pulse SILAC in human erythroblasts at day 10 (proE/baso1). Cells were cytokine-starved for 4 hours before incubation in SILAC medium with 10 UI/mL EPO, 100 ng/mL SCF, or EPO+SCF, in the presence or absence of 2 μM of the c-Kit inhibitor masitinib for 24 hours. For each experiment, the median of neosynthesized RP percentages was determined. Results are shown as means ± SEM of 3 independent experiments. **$P < .01$, by Student *t* test. (L) Cytology of sorted human proEs/baso1 (GlyA^{low}/Band3$^-$) and baso2 (GlyA^{high}/Band3$^+$) after May-Grünwald-Giemsa staining. Original magnification ×100. (M) Ribosome neosynthesis by pulse SILAC of sorted human erythroblasts GlyA^{low}/Band3$^-$ and GlyA^{high}/Band3$^+$ incubated in SILAC medium with EPO+SCF for 24 hours. Results representative of 1 experiment and expressed as the median of neosynthesized RP percentages are shown.

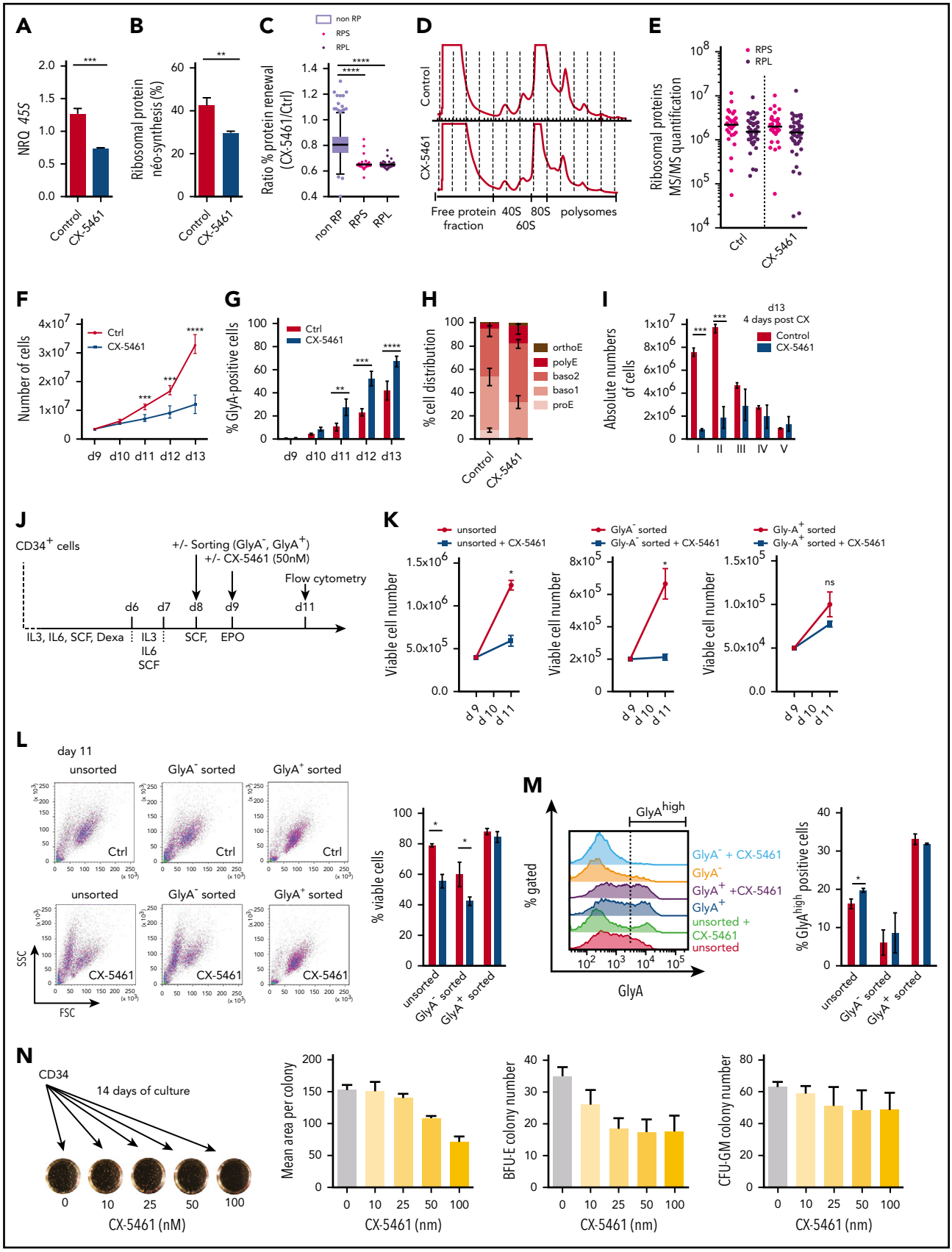

Figure 2. Inhibition of RNA Pol I by CX-5461 decreases the proliferation of immature erythroblasts. Human primary erythroblasts were derived from CD34+ progenitors cultured for 6 days with SCF, IL-6, IL-3, and dexamethasone; for 1 day with SCF, IL-6, and IL-3; for 4 days between days 7 and 11 with SCF and EPO; and then with EPO alone. CX-5461 (50 nM) was added to erythroblast cultures at day 9. (A) Quantification by qRT-PCR of pre-rRNA 45S transcript after 48 hours of treatment with CX-5461. Transcripts amounts

by standardization to the total histone mass spectrometry (MS) signal.[24]

Short hairpin RNA and cell transduction

pH1 short hairpin RNA (shRNA) p53 cloned into the pRRL-PGK-GFP lentiviral vector and control sh scrambled (SCR) RNA were kindly provided by I. Plo (Gustave Roussy, Villejuif, France).[25] In brief, CD34$^+$ cells were cultured for 6 days with interleukin-3 (IL-3), IL-6, SCF, with dexamethasone added on day 1; SCF and EPO on day 7; and then EPO alone on day 12. Erythroblasts were transduced twice, at day 8 and 9, with 2 μL lentiviral supernatant. Forty-eight hours after the first transduction, GFP expression, as analyzed by flow cytometry, was >95%.

Tp53-deficient mice

Mice carrying the p53-knockout allele were obtained from The Jackson Laboratory (Ellsworth, ME) (supplemental Material).[26] At 6 to 8 weeks old, FVB/N *Tp53*$^{-/-}$ mice were treated with CX-5461 (40 mg/kg) by oral gavage. After 24 hours, blood counts were measured, the mice were euthanized, and bone marrow cells were harvested for analysis.

Western blot and immunofluorescence

Antibodies used are listed in supplemental Table 2 and the supplemental Material.

Chromatin immunoprecipitation-sequencing bioinformatics analysis

p53 chromatin immunoprecipitation-sequencing (ChIP-seq) was performed as previously described[27,28] (supplemental Material). Sequence reads were mapped by using Bowtie (v2.3.4.3) against the human genome hg19 assembly (Genome Reference Consortium Human Build 37) downloaded from the University of California Santa Cruz (UCSC) Genome Browser (http://genome.ucsc.edu). Alignment files were converted into bam files by using Samtools (v1.9). Mapped reads (sequences) were transformed into a genome-wide read density (coverage) by bamCoverage (v3.3.0) from the deepTools suite using the parameter "normalize using RPKM" to normalize the number of reads per bin to the number per kilobase per million mapped reads. Peak calling was performed with Homer (v4.10, 16 May 2018), with default parameters. Published data sets used in this study (GATA1, H3K27Ac, H3K27me3, H3K4me3, and RNAPII) were downloaded from the Gene Expression Omnibus public database (accession codes: GSE36985 and GSE70660).

Statistical analysis

For quantitative variables, values are expressed as means and standard error of the mean (SEM) and compared by Student *t* test. Correlations were determined by the Pearson test. $P < .05$ indicates statistical significance (Prism 7.0; GraphPad, San Diego, CA).

Results

Dynamic changes of ribosome biogenesis during erythroid differentiation

Ribosome clearance associated with erythroid maturation has been estimated by establishing the ribosome quantities at each developmental stage.[15,20,21] Here, we investigated the dynamics of ribosome renewal by following the kinetics of rRNA expression and the incorporation of RPs into the ribosome during both human and murine erythroid differentiation. Primary erythroblasts were expanded from CD34$^+$ progenitors isolated from human cord blood. Cells proliferated until day 19, their expression of c-Kit/CD117 decreased, and their number was reduced from day 13 as they differentiated into mature polyEs and orthoEs (Figures 1A-C). In vitro differentiation of murine erythroblasts was obtained by expanding ESREs from fetal liver. Within 3 days, the proliferation rate increased by ninefold. From day 2, the cells lost c-Kit expression, adopted polyE and then orthoE morphology, and expressed β-globin (supplemental Figures 1A-D). We evaluated the cellular ribosome content by measuring RNA quantities, mainly composed of 28S and 18S rRNA. Ribosomal fractions were purified from human erythroblasts or murine ESREs. In human erythroblast cultures, RNA quantities strongly decreased (Figure 1D) in correlation with the disappearace of immature erythroblasts (Spearman's test; $r = 1$; $P < .0001$). By qRT-PCR, we showed that the quantities of rRNA precursor 45S were significantly downregulated at day 16 of culture concomitantly with the upregulation of β-globin mRNA (Figure 1E; top). The 45S rRNA revealed by fluorescence in situ hybridization was no longer detected in the nucleus of orthoEs at day 19, suggesting that ribosome biogenesis stopped after the baso2 stage (Figure 1E, bottom). In murine ESREs, rRNA quantities normalized to cell number decreased at day 2 after induction of maturation (supplemental Figure 1E).

We then reanalyzed the expression of RPs in our published proteomic data obtained from human primary erythroblasts.[20] Absolute quantification of RPs normalized to histones on total

Figure 2 (continued) were normalized to *B2M*, *UBC*, and *ACTB* and expressed as the normalized relative quantity (NRQ). Mean NRQ ± SEM of 3 experiments. (B) Percentage of RP neosynthesis after SILAC labeling of human erythroblasts for 48 hours in the presence or absence of CX-5461. Results are expressed as the mean ± SEM of 3 experiments. (C) Comparison of the ratios of non-RP, RPS, and RPL neosynthesis after SILAC between CX-5461-treated and untreated cells. Results are expressed as means ± SEM of 3 independent experiments. (D) Polysome profiling. Ribosomes from human erythroblasts, treated or not with CX-5461 for 48 hours, were purified on sucrose gradient, and the relative abundance of free-RNP complexes; the 40S, 60S, and 80S subunits; and polysomes were measured by absorbance at OD 260 nm. (E) Label-free proteomic for absolute quantification of RPs by mass spectrometry after 48 hours of incubation, with or without CX-5461. Results are expressed as the mean copy number ± SEM of 5 independent experiments. (F) Proliferation rate of human erythroblasts expressed as the cumulative number of cells at each time point. Mean ± SEM of 4 experiments. (G) Percentages of GlyA$^+$ cells were quantified by flow cytometry and are shown as the mean ± SEM of 4 experiments. (H) Proportions of erythroid precursor populations at day 13 by cytological examination of May-Grünwald-Giemsa–stained cytospins. Mean percentages ± SEM of 4 experiments. (I) Flow cytometry of α4 integrin/CD49d and Band3 expression in GlyA$^+$ cells identifying proE (I), baso1 (II), baso2 (III), polyE (IV), and orthoE (V) cells according to Hu et al.[3] Absolute number of each precursor is shown as the mean ± SEM of 3 experiments. (J) Timeline of sorting of GlyA$^-$ (progenitor) and GlyA$^+$ immature precursors (proE) at day 8. CX-5461 (50 nM) was added at day 9 for 48 hours, and the cells were analyzed at day 11. (K) Absolute number (means ± SEM of 3 experiments) of unsorted cells (left), progenitors (progs; middle), and proEs (right). (L) Flow cytometry histograms (side scatter [SSC]/forward scatter [FSC]) for percentages of viable cells (means ± SEM of 3 experiments). (M) Flow cytometry histograms of GlyA expression (left) expressed as mean percentages ± SEM of GlyA$^+$ cells (right). (L-M) Control: red bars; CX-5461: blue bars. (N) Colony assays. Cord blood–derived CD34$^+$ progenitors were seeded for 14 days in methylcellulose with increasing concentrations of CX-5461 (left). Colony area and counts were determined and are represented as means ± SEM of 3 independent experiments (right). For all panels: *$P < .05$; **$P < .01$; ***$P < .001$; ****$P < .0001$, by Student *t* test.

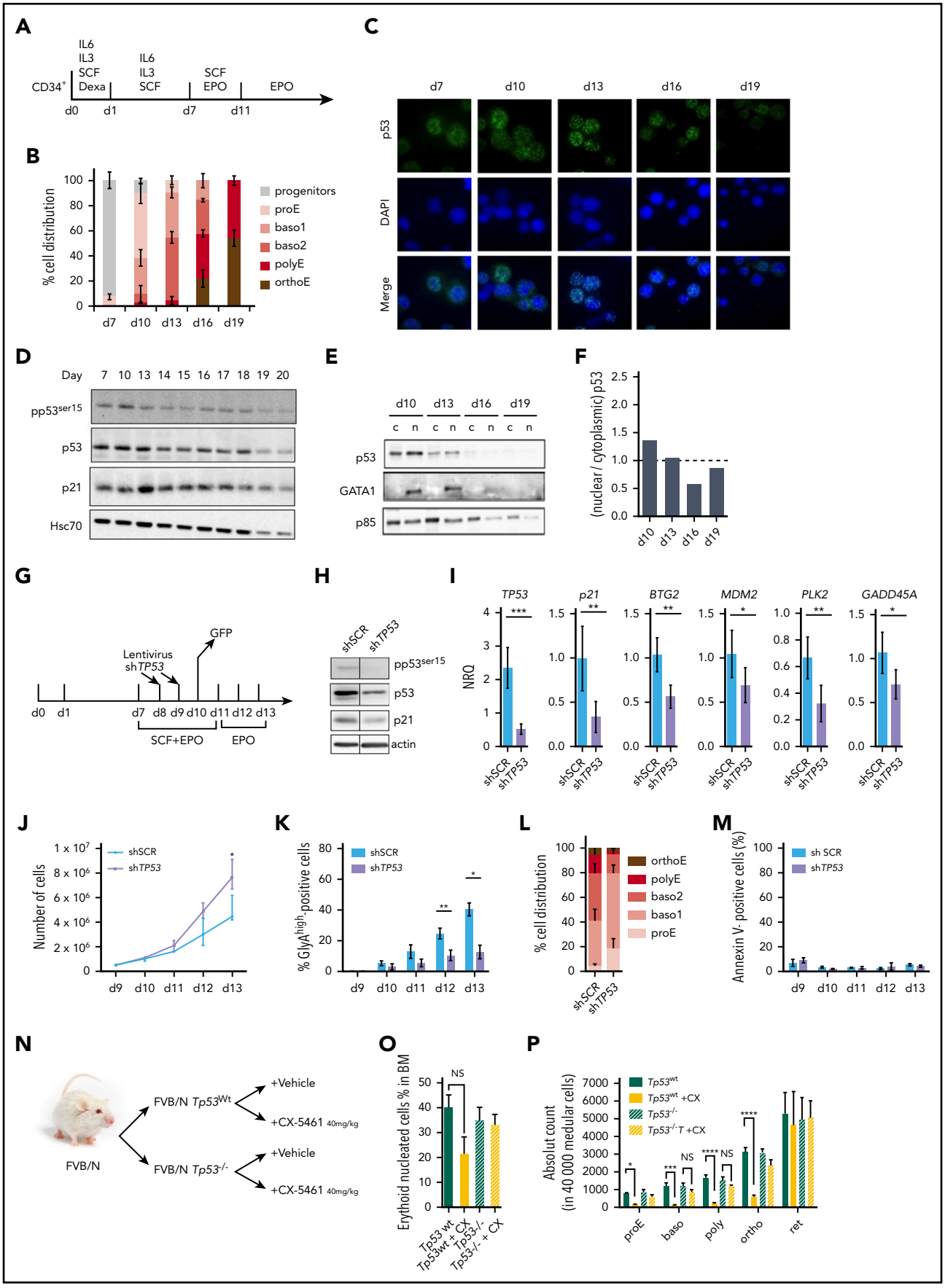

Figure 3.

cell lysates indicated that the mean protein copy number per cell of RPSs or RPLs underwent a threefold decrease in baso2 and a 10-fold decrease in orthoEs compared with proEs and baso1 (Figure 1F). The ribosome content was therefore lower in mature compared with immature erythroblasts. To investigate whether the changes in ribosome content were governed by variations in ribosome biogenesis, we next measured the dynamics of ribosome neosynthesis using the pulsed stable isotope labeling by amino acids in cell culture (SILAC) method on different days of culture.[29] After metabolic labeling, the ribosomes were purified and trypsin-digested peptides were analyzed by liquid chromatography-tandem mass spectrometry (LC-MS/MS; Figure 1G). We identified 34 and 33 RPSs and 43 and 46 RPLs in human and murine cells, respectively, with more than 2 peptides and 15% of sequence coverage (supplemental Figure 2A; supplemental Tables 3-4). In human cells, the proportion of neosynthesized RP incorporated in the ribosome calculated as the ratio of newly synthesized heavy (H) RPs to the sum of heavy plus preexisting light (L) RPs ([H/H+L] × 100) was maximal (54%) at day 10, when 90% of erythroblasts were immature, started to decrease at day 16, and collapsed down to 11% at day 19 when >70% of erythroblasts were mature (Figure 1H). In murine ESREs, the proportion of neosynthesized RPs declined sharply after 2 days of terminal differentiation (supplemental Figure 1F). The renewal of each RPL or RPS decreased similarly during the differentiation from day 16 of culture (Figure 1I). To obtain a more detailed understanding, we quantified the rate of incorporation of each newly synthesized RP in the ribosome by normalizing the H/L ratio to the median of H/L ratios of all RPs in a given subunit. Representative heat maps show that the incorporation rate of neosynthesized RP could vary depending on the protein (Figure 1J; supplemental Figure 1G).

Ribosome neosynthesis correlated very well with the proportion of proEs (Spearman's test; $r = 0.894$; $P = .038$) and its decrease was concomitant with the diminution of c-Kit/CD117 expression in human erythroblasts at day 16 and in murine ESREs at day 2 (Figure 1B; supplemental Figure 1D). Thus, we hypothesized that the variations of ribosome biogenesis between immature (proEs/baso1s) and mature (baso2s/polyEs) erythroblasts could be under the extrinsic control of SCF. To support this thesis, SILAC was performed in human immature erythroblasts incubated with EPO 1 UI/mL, SCF 100 ng/mL, or both cytokines. The proportion of neosynthesized ribosome was 50% with SCF and EPO, but was reduced by half when the cytokines were added individually, demonstrating a significant additive effect of SCF and EPO (Student *t* test; $P < .01$). Ribosome neosynthesis was >20% in the presence of masitinib (2 μM), a potent inhibitor of c-Kit tyrosine kinase, and was reduced in sorted mature glycophorin A (GlyA)^{high}Band3^{+} (baso2) cells compared with immature GlyA^{low}Band3^{-} cells (proEs/baso1; Figures 1K-M). Taken together, the results show that a decrease in ribosome content in mature erythroblasts is initiated by a balanced inhibition of RP neosynthesis and incorporation into the ribosome, which correlates, with the loss of response to SCF of mature erythroblasts.

Inhibition of ribosome biogenesis by CX-5461 restrains immature erythroblast proliferation

To investigate the consequences of inhibiting RP neosynthesis during erythroid differentiation, we prematurely arrested ribosome biogenesis in proEs and baso1s using CX-5461, a specific RNA Pol I inhibitor.[30] CX-5461 (50 nM) decreased the expression of 45S rRNA precursor (Figure 2A), whereas the expression of RP mRNA was not affected (supplemental Figure 2B). A 30% reduction of ribosome neosynthesis was noted after a 24-hour SILAC pulse (Figure 2B), and RP neosynthesis was specifically affected compared with that of other proteins that purified with the ribosome and represented the ribointeractome (Figure 2C).[29] The ribosome profile showed that the distribution of ribosomal subunits among the free ribosomal subunits 40S and 60S, assembled 80S, and polysomes was mostly unchanged after 48 hours of treatment (Figure 2D), and consistently, the ratio of mean copy number per cell of each RP normalized to histone signal remained stable after 48 (Figure 2E) or 96 hours of treatment with CX-5461 (supplemental Figure 2C). Importantly, the quantity of RPs in the free protein fraction expressed as a ratio of intensities in CX-5461-treated relative to control conditions did not increase. These findings imply that the extinction of ribosome biogenesis by CX-5461 did not lead to accumulation of free RPs (supplemental Figure 2D).

Cell proliferation decreased significantly at 3 days after treatment with CX-5461 with >20% of apoptotic cells, even after 4 days (Figures 2F; supplemental Figure 3A). In the presence of CX-5461, cultures were at a later stage of development, with enrichment of mature erythroblasts as monitored by increased percentage of GlyA^{+} cells from day 11, 48 hours after addition of CX-5461 (Student *t* test; $P < .001$; Figure 2G). Cytological examination confirmed the enrichment in polyEs and orthoEs and quantitative proteomics showed a 1.5- to 4-fold increase

Figure 3. p53 is activated during erythroid differentiation. (A) Human primary erythroblasts were derived from CD34^{+} progenitors cultured with SCF, IL-6, and IL-3 for 6 days (with the addition of dexamethasone at day 1); with SCF and EPO between days 7 and 11; and then with EPO alone. (B) Proportion of progenitors, ProEs, baso1s, baso2s, polyEs, and orthoEs by cytological examination of May-Grünwald-Giemsa–stained cytospins. Mean ± SEM of 3 independent experiments. (C) Expression of the SCF receptor CD117 and GlyA by flow cytometry during human erythroblast differentiation. p53 expression in human primary erythroblasts at different days in culture by immunofluorescence imaging of p53 and 4′,6-diamidino-2-phenylindole (DAPI) staining, with merged images of the 2 stains. Images were obtained on a Leica DMI6000 inverted microscope with spinning disk and analyzed with ImageJ. Original magnification ×100. (D) Western blot analysis of phospho-p53 serine 15 (pp53^{ser15}), p53, and p53 target p21/Cdkn1A during normal erythroblast differentiation. Hsc70 was used as the loading control. (E) Western blot analysis of p53 in nuclear and cytosolic fractions. GATA1 was used as the loading control for the nuclear fraction (n), and the p85 subunit of phosphatidylinositol 3 kinase was used as the loading control for the cytosolic fraction (c). (F) Quantification of nuclear and cytoplasmic expression of p53 is expressed as the nuclear/cytoplasmic ratio. (G) Timeline of GFP-shRNA lentivirus transduction at days 8 and 9 and control of GFP expression at day 10. Cells were analyzed during the 4 days after the last transduction (day 13). (H) Western blot analysis of *TP53* knockdown by shRNA at day 13. An SCR shRNA was the control. pp53^{ser15}, p53, and p21/Cdkn1A protein expression are shown. Actin was used as the loading control. (H) Erythroid differentiation was assessed by the quantification of GlyA expression by flow cytometry. Results are expressed as mean percentages ± SEM of 3 experiments. (I) qRT-PCR measurement of p53 target genes quantities in sh*TP53* and shSCR erythroblasts. Transcript levels were normalized to *B2M*, *UBC*, and *ACTB* levels. Results are expressed as mean NRQs ± SEM of 3 experiments. (J) Proliferation curve of sh*TP53* and shSCR erythroblasts in a cumulative number of cells. (K) GlyA expression in sh*TP53* and shSCR erythroblasts. Mean percentages ± SEM of 3 experiments. (L) Proportions of erythroblasts by cytological examination of May-Grünwald Giemsa–stained cytospins at day 13. Mean percentage ± SEM of 3 experiments. (M) Apoptosis measured as the mean percentage ± SEM of annexin V^{+} cells in 3 experiments. (N) Design of mouse experiments. FVB/N *Tp53*$^{-/-}$ or *Tp53*^{wt} mice were treated with 40 mg/kg CX-5461 for 24 hours. (O-P) Bone marrows were collected and the percentage of erythroid nucleated cells (O) and the absolute number of proE, baso, poly, ortho, and reticulocytes (P) were determined by flow cytometry. *$P < .05$; **$P < .01$; ***$P < .001$, by Student *t* test.

of the major erythroid protein copy number after CX-5461 treatment (Figure 2H; supplemental Figures 3B-C). To discriminate between induction of differentiation or selection of mature cell populations, we used flow cytometry to identify erythroid precursor subpopulations among GlyA^{+} cells.[3] The results clearly indicated decreased absolute numbers of GlyA^{low}CD49d^{hi}Band3^{neg} (proEs) and GlyA^{low}CD49d^{hi}Band3^{low} (baso1) after 4 days of treatment with CX-5461 (day 13), whereas the absolute number of GlyA^{hi}CD49d^{hi}Band3^{med} (baso2), GlyA^{hi}CD49d^{med}Band3^{hi} (polyEs), and GlyA^{hi}CD49d^{low} Band3^{hi} (orthoEs) remained unchanged (Figure 2I; supplemental Figures 3D-E). GATA1 mRNA and protein expression remained stable, whereas gene set enrichment analysis (GSEA) from transcriptomic data demonstrated a significant upregulation of GATA1 targets when mature erythroblasts were enriched after 2 days of CX-5461 treatment (supplemental Figures 3F-H; supplemental Table 5). Thus, the inhibition of ribosome biogenesis by CX-5461 could restrain the proliferation of immature erythroblasts but spare mature erythroblasts. To confirm this observation, we sorted GlyA^{+} and GlyA^{-} cells in culture at day 8 and treated them from days 9 to 11 with CX-5461 (50 nM; Figure 2J). The number and percentage of viable cells were significantly decreased in unsorted and GlyA^{-} progenitors but not significantly in GlyA^{+} sorted cells (Figures 2K-L). The percentage of GlyA^{+} cells was not affected after 2 days in cultures derived from GlyA^{-} or GlyA^{+} sorted fractions (Figure 2M). Finally, we evaluated the effect of increasing concentrations of CX-5461 on the growth of erythroid progenitors (BFU-E) as compared with that of colony forming unit-granulomonocyte (CFU-GM) progenitors. The size of all types of colonies was diminished at day 14 in the presence of 50 nM CX-5461 or higher concentrations. In addition, the number of BFU-E colonies decreased in a dose-dependent manner, with a plateau value reached at 25 nM of CX-5461, whereas the number of CFU-GM progenitors remained unchanged at all concentrations used (Figure 2N). These findings confirm that CX-5461 preferentially targets erythroid progenitors and immature precursors that require active ribosome biogenesis for their proliferation.

p53 activation coincides with a decrease in ribosome biogenesis

The haploinsufficiency of specific ribosomal protein genes and unbalanced ribosome biogenesis perturbed ribosome homeostasis and resulted in p53 activation that drove cell cycle arrest and apoptosis of erythroblasts. Whether the disruption of ribosome biogenesis during normal erythroid differentiation is also associated with p53 activation was investigated. Using a culture system with only 1 day of dexamethasone, which slightly accelerates differentiation (Figures 3A-B), we studied the expression and localization of p53 in human erythroblasts by immunofluorescence microscopy. p53 was expressed in the nucleus and cytoplasm of erythroblasts at different developmental stages and was more abundant in the nucleus on days 10 and 13 (Figure 3C). By western blot analysis, p53 was shown to be transiently phosphorylated on serine 15 at day 10 (Figure 3D), whereas its global expression remained unchanged. The expression of its transcriptional target p21/Cdkn1A overlapped with that of p53 but not of pp53 expression, suggesting that there is an alternative mechanism of p21 regulation. Because the phosphorylation signal was faint, we performed cell fractionation to study p53 expression in the nuclear fractions. As shown in Figure 3E-F, p53 was expressed in the nucleus at days 10 and 13 with a nucleocytoplasmic ratio >1.

To investigate the role of p53 in erythroid differentiation, we transduced primary erythroblasts with a lentiviral vector encoding an shRNA to *TP53* at days 8 and 9 of culture and monitored their differentiation (Figure 3G). This shRNA efficiently reduced p53 expression and p21 expression and abrogated the detection of phospho-p53 (Figure 3H). p53 transcriptional targets were significantly downregulated (Figure 3I). The proliferation capacities of sh*TP53* erythroblasts were significantly increased (Figure 3J), whereas their capacity to differentiate was altered, with a reduced percentage of GlyA^{+} cells at days 12 and 13 and an accumulation of baso1 at day 16 (Figures 3K-L). No sign of apoptosis was evidenced (Figure 3M). These results imply that p53 is essential, either to restrain immature erythroblast proliferation or to induce their differentiation. To discriminate between those 2 hypotheses, we studied erythropoiesis of *Tp53*$^{-/-}$ mice (Figure 3N). Hemogram parameters such as number of red cells, hemoglobin level, hematocrit, mean corpuscular volume, and spleen weight were similar between *Tp53*$^{-/-}$ and *Tp53*^{wt} mice (supplemental Figure 4A). Flow cytometry revealed that, in the bone marrow, the absolute numbers of nucleated erythroblasts, proEs, basoEs, polyEs, orthoEs, and reticulocytes were similar in these homeostatic steady-state conditions (supplemental Figure 4B; Figures 3O-P). We then explored the in vivo effects of CX-5461 on erythropoiesis in *Tp53*$^{-/-}$ and *Tp53*^{wt} mice. CX-5461 was administered orally at a dose of 40 mg/kg, and hematopoiesis was studied 24 hours later, to ensure completion of murine erythroid differentiation. Within this period, no stress erythropoiesis was induced in the spleen. CX-5461 potently decreased the number of bone marrow erythroid precursors of *Tp53*^{wt} but not of *Tp53*$^{-/-}$ mice. Thus, CX-5461 inhibited the proliferation of erythroblasts in a p53-dependent manner. Altogether, these results indicate that p53 could be necessary to restrain the proliferation of immature erythroblasts and thereby facilitate their entry into the final steps of maturation.

A p53-dependent transcriptional program is activated during erythroid differentiation

To better understand the consequences of p53 activation during erythroid precursor maturation, we analyzed p53 direct targets by immunoprecipitating p53 on the chromatin followed by sequencing (ChIP-seq). Erythroblasts were collected at day 11, and those immature erythroblasts were compared with mature erythroblasts enriched by a 2-day treatment with CX-5461 at days 9 and 10. As already shown in Myc-driven lymphoma,[30] addition of CX-5461 at a concentration of 50 nM induced p53 phosphorylation and upregulation of p21 expression, although the quantity of p53 protein remained constant (Figure 4A). GSEA of the transcriptome showed an enrichment of the *TP53* pathway gene set (normalized enrichment score, 2.39; $P = .001$; Figure 4B; supplemental Table 6). Positive regulation of cell cycle arrest, negative regulation of apoptotic process, and DNA damage response (DDR) were among the most significantly upregulated Gene Ontology (GO) terms with a 1.2-fold change (Figure 4C). By ChIP-seq experiments, 8108 p53-bound regions were detected, corresponding to 4257 genes in erythroblasts without CX-5461, whereas only 3095 peaks (corresponding to 1203 genes) were detected in treated conditions, including 1888 peaks shared by the 2 conditions, corresponding to 692 genes.

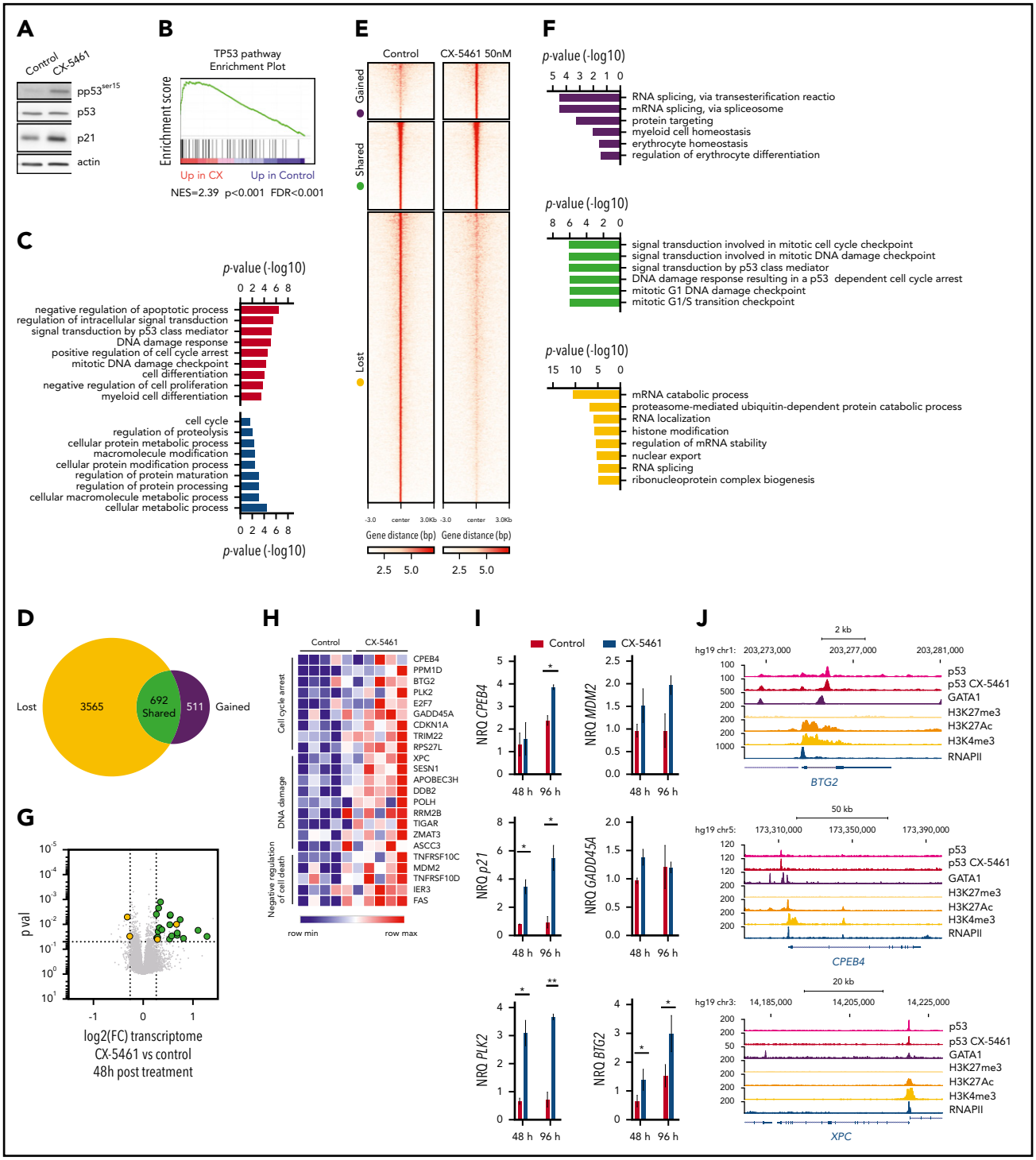

Figure 4. Activation of a p53-dependent transcriptional program during erythroid differentiation. Human primary erythroblasts were cultured with SCF, IL-6, and IL-3 for 6 days (with the addition of dexamethasone at day 1) and then with SCF and EPO between days 7 and 11. CX-5461 (50 nM) was added at day 9 for 48 hours, and control or treated cells were collected at day 11. (A) Western blot showing p53 activation by CX-5461. Actin was used as the loading control. Representative results of 3 independent experiments. (B) GSEA of p53 pathway genes in erythroblasts treated by CX-5461 or vehicle. NES, normalized enrichment score. (C) GO term enrichment analysis of differentially expressed genes between treated and untreated erythroblasts with CX-5461 for 48 hours. (D) Venn diagram of the repartition of p53 direct target genes identified by ChIP-seq in CX-treated and control erythroblasts. Lost, control; shared, control or CX-5461; gained, CX-5461. (E) ChIP-seq density heat maps showing the landscape of p53 target genes in control and CX-5461 treatment conditions. (F) GO analysis of the 70 upregulated p53 direct target genes after CX-5461 treatment. (G) Volcano plot representing p53 targets identified by ChIP-seq, either shared by control and CX-5461 treatment conditions (green) or detected in control conditions (yellow), the expression of which in log2 (FC) is upregulated by CX-5461. FC, fold change. (H) Heat map visualization of the most representative p53 direct target genes upregulated after CX-5461 treatment. (I) Quantification of p53 direct target gene expression after 48 and 96 hours of CX-5461 treatment by qRT-PCR. *$P < .05$, **$P < .01$, by Student t test. (J) Combined analysis of p53 peaks in selected genes in control and CX-5461 treatment conditions and GATA1, H3K27me3, H3K27, H3K4me3, and RNA Pol II (RNAPII) peaks identified in human proEs by Xu et al[31] and Huang et al.[32]

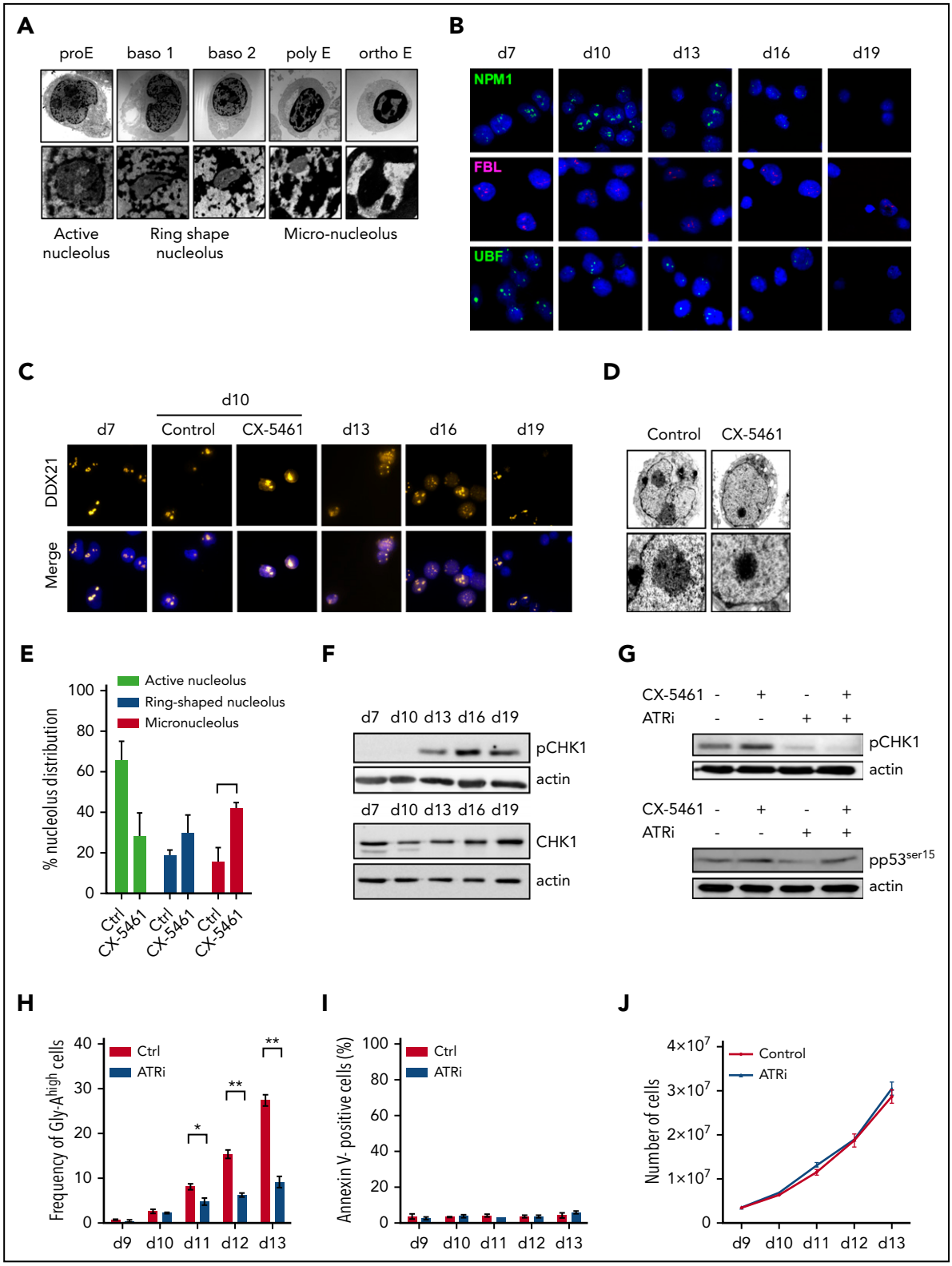

Figure 5. RNA Pol I complex disruption and ATR-CHK1-p53 pathway activation. Human primary erythroblasts were derived from CD34^{+} progenitors cultured with SCF, IL-6, and IL-3 for 6 days (with the addition of dexamethasone at day 1); SCF and EPO between days 7 and 11; and then EPO alone. (A) TEM analysis of nucleolus structure in human erythroblasts during in vitro differentiation. Original magnification ×4000 (top); ×24 000 (bottom). (B) Representative immunofluorescence images of nucleolar compartments during erythroid differentiation. NPM1, FBL, and UBF were used as markers of the granular component, dense fibrillar component, and fibrillar center, respectively. (C) Representative immunofluorescence images of DDX21 nucleolar delocalization in differentiating erythroblasts, and CX-5461 (50 nM for 48 hours)-treated erythroblasts. (B-C) Micrographs were obtained on a Leica DMI6000 inverted microscope with spinning disk and analyzed with ImageJ. Original magnification ×100. (D) TEM analysis of nucleolus structure in human pro-erythroblasts untreated or treated with CX-5461 (50 nM) for 48 hours. Original magnification ×6000 (top); ×24 000 (bottom). (E) Proportion of active, ring-shaped, and micronucleolar cells in control and CX-5461 treatment conditions. More than 100 nucleoli were analyzed in 3 separate experiments. Mean percentages ± SD.

These results suggest that p53 binding to the chromatin could decrease at a stage where mature erythroblasts are enriched in the presence of CX-5461 (Figures 4D-E). A GO term enrichment analysis revealed that p53-bound regions belong to genes involved in distinct cellular pathways in control cells, CX-5461-treated cells, or both (Figure 4F). Combining ChIP-seq and transcriptomic data showed that genes that were significantly upregulated after CX-5461 treatment belonged to the set of p53-bound genes shared by control and CX-5461 treatment conditions and were implicated in cell cycle regulation, negative regulation of cell death, and DDR (Figures 4G-H). Using qRT-PCR, we confirmed that the expression of the p53 target genes B-cell translocation gene antiproliferative factor 2 (*BTG2*) and cytoplasmic polyadenylation element binding factor 4 (*CPEB4*) increased with time in differentiating erythroblasts and further increased in CX-5461-treated conditions, together with the *p21/CDKN1A*, *PLK2*, *GADD45A*, and *MDM2* genes (Figure 4I).

Finally, integration of published epigenetic and GATA1 ChIP-seq data from Xu et al[31] and Huang et al [32] showed that p53 target genes may be GATA1 targets and present with an open chromatin mark (Figure 4J; supplemental Figure 5A). Among the p53 targets upregulated during erythroid differentiation, some presented strong GATA1 binding sites close to such p53 binding sites as *BTG2*, *CPEB4*, and *XPC*. The distance between p53 and GATA1 peak summits was 250 bp at the *BTG2* locus, 500 bp at the *CPEB4* locus, and 81 bp at the *XPC* locus. Others, such as *XPC* or *MDM2*, appeared to be more p53-specific targets with minimal GATA1 signals close to p53 sites (supplemental Figure 5B). This result indicates that p53-bound regions, although not directly overlapping with GATA1, were frequently located in the vicinity of GATA1 sites. To better estimate the direct overlap of p53 and GATA1 peaks, we considered p53 peaks extending from the summit ±3 kb, with GATA1 peaks with at least a 1-bp overlap between the covered DNA regions (supplemental Figures 5C). Using this method, we found 3917 (56%) overlapping peaks among 7004 p53 peaks detected without CX-5461 (lost), 1009 (49%) overlapping peaks among 2069 p53 peaks detected both in the absence and presence of CX-5461 (shared), and 796 (58%) overlapping peaks among 1365 p53 peaks detected at a stage where mature erythroblasts were enriched in the presence of CX-5461 (gained; supplemental Figure 5D). Measurement of the distance between p53 and GATA1 peaks showed that most of them were separated by >1 kb (supplemental Figures 5E-F).

These data suggest that erythroid differentiation could result from the combined action of p53 and GATA1 regulatory pathways in some erythroid genes.

Erythroid differentiation recapitulates nucleolar stress, leading to ATR-CHK1-p53 pathway activation

Transmission electron microscopy (TEM) imaging of primary human erythroblasts collected by sternal aspiration demonstrated that the cells underwent nuclear condensation and nucleolar disruption during maturation (supplemental Figure 6A). In vitro differentiation of erythroblasts recapitulated these nucleolar changes, showing active nucleoli in 100% of proEs and 82% of baso1, ring-shaped nucleoli in 31% of polyEs, and micronucleoli or no nucleoli in orthoEs (Figure 5A; supplemental Table 7). Active nucleoli are composed of a fibrillar center (FC) labeled by upstream binding transcription factor (UBF), a dense fibrillar component (DFC) labeled by fibrillarin (FBL), and a granular component (GC) labeled by nucleophosmin (NPM1). The border between FC and DFC, which changes in volume and number during erythropoiesis, is the site of rRNA transcription and early processing.[33] Immunofluorescence detection of NPM1, UBF, and FBL showed a reduction of signal intensities in polyEs compared with immature erythroblasts and an extinction of FBL and UBF in orthoE corresponding to the exclusion of FC and DFC (Figure 5B).

The nucleolar DEAD-box RNA helicase DDX21 has been shown to be involved in the regulation of rRNA synthesis, and processing and its depletion from the nucleolus coincides with arrest of RNA Pol I machinery and is a marker of nucleolar stress.[34] Immunofluorescence experiments revealed that DDX21 relocalized to the nucleoplasm at day 13 corresponding to a stage were basophilic erythroblasts were enriched. DDX21 also exited from the nucleolus upon acute inhibition of RNA Pol I by CX-5461 (Figure 5C). As shown by TEM imaging, CX-5461 strongly affected the morphological features of nucleoli (Figure 5D), resembling those induced by actinomycin D, which inhibited RNA Pol I transcription at the level of elongation (supplemental Figure 6B). We quantified the proportion of each nucleolus type and found that multiple active nucleoli decreased in favor of single or ring-shaped nucleoli or micronucleoli, consistent with a nucleolar disruption mimicking that of differentiated erythroblasts, even if the chromatin was not condensed (Figures 5E).

Concomitant to this nucleolar stress, we noted phosphorylation of checkpoint kinase-1 (CHK1) suggesting that the Ataxia telangiectasia and Rad3 (ATR)-CHK1 pathway was activated (Figure 5F). Its phosphorylation was also triggered after CX-5461 treatment. To further investigate this pathway, we treated erythroblasts with the ATR inhibitor (ATRi) VE-821,[35] and noted that VE-821 inhibited the phosphorylation of CHK1 on serine 345 and p53 on serine 15, suggesting that this pathway could be responsible, at least in part, for p53 activation in this context (Figure 5G). Finally, the ATRi reduced the proportion of mature erythroblasts, whereas it maintained a normal rate of proliferation without any sign of apoptosis (Figures 5H-J). Our results imply a role for the ATR-CHK1 pathway in the activation of p53.

Discussion

Our findings provide a comprehensive characterization of ribosome biogenesis dynamics during erythropoiesis, by showing that (1) ribosome biogenesis participates in the control of transition between proliferation and differentiation; (2) p53

Figure 5 (continued) (F) Western blot of phospho-CHK1 serine 345 (pCHK1) and CHK1 during normal erythroid differentiation. (G) The ATR inhibitor (ATRi) VE-821 (1 μM), CX-5461 (50 nM), or both were added to erythroblasts at day 9 for 48 hours. pCHK1 expression by western blot (top) and pp53^{ser15} expression (bottom). Actin was the loading control. Representative immunoblots of 3 independent experiments. (H) ATRi VE-821 was added to erythroblasts at day 9 for 4 days. GlyA expression was quantified by flow cytometry. Mean percentage ± SEM of 3 experiments. (I) Number of annexin V$^+$ cells. Mean percentage ± SEM of 3 experiments. (J) Proliferation curves. Mean cumulative number of cells ± SEM of 3 experiments.

activation is involved in the control of immature erythroblast proliferation; and (3) activation of ATR-CHK1-p53 pathway results from a RNA Pol I transcriptional stress.

We further documented that c-Kit signaling is critical for optimal ribosome neosynthesis, suggesting that the maintenance of cell proliferation by SCF is dependent on the stimulation of ribosome biogenesis. We also showed that ribosome biogenesis is abruptly interrupted by the decrease in rDNA transcription, a rate-limiting factor for ribosome biogenesis. Although RP transcript expression remains stable until the polyE stage,[6] the absolute quantities of ribosomal proteins significantly decreased between the baso1 and baso2 stages concomitant with decrease in cell size. This effect resulted from the decrease in neosynthesis and possibly an increase in degradation, which we cannot exclude. Furthermore, the pool of preexisting ribosomes was divided between 2 daughter cells, resulting in reduction by half of RP protein copy number per cell between baso2 and polyE and between polyE and orthoE. Thus, the decrease in ribosome content was caused by both biogenesis arrest and cell division. In ribosomopathies, the production of RPs is unbalanced, leading to free RPL11 and RPL5 accumulation[36-38] and finally to p53 stabilization and activation, cell cycle arrest, and apoptosis.[18,19,39-41] In normal or CX-5461-treated erythroblasts, we did not detect accumulation of free RPs, making inhibition of MDM2 and stabilization of p53 unlikely.

Nevertheless, p53 was activated through its phosphorylation in immature erythroblasts or CX-5461-treated erythroblasts. Although p53 appears to be dispensable for homeostatic erythropoiesis in mice, in conditions of stress erythropoiesis induced by dexamethasone on fetal liver cells or by phenylhydrazine-induced hemolytic anemia, the absence of p53 increases the proliferation of erythroid progenitors and immature precursors.[42] Our experiments further suggest a role for p53 in the control of progenitor and immature erythroid precursor proliferation. Similar to nonapoptotic activation of caspases, which is necessary for normal erythroid differentiation,[43] a p53-dependent program associating cell cycle arrest (*CDKN1A*, *PLK2*), negative regulation of apoptosis (*FAS*, *IER3*), and DNA damage response (*XPC*, *DDB2*) could be involved in erythroid differentiation. Notably, 2 proapoptotic effectors of the DDR, *PUMA/BBC3* and *NOXA/PMAIP1*, which are p53 targets, were not upregulated, suggesting that p53 activation is selective.[44] Interestingly, some genes, such as p21/CDKN1A, are common targets of p53 and GATA1.[45] Others, such as *BTG2* and *CPEB4*, present with open chromatin marks in p53-bound regions and usually with a GATA1 binding site in proximity, suggesting that a coregulation of gene expression implicating both transcription factors could occur.[46] Therefore, we do not exclude that the erythroid transcriptional program is remodeled as the result of p53 and GATA1 interaction. Previous work has shown that GATA1 has an inhibitory interaction with p53.[47]

Changes in ribosome biogenesis are concomitant with the loss of Myc, Spi-1/PU.1, and Fli-1, known as direct transcriptional activators of both rDNA and RP gene transcription and/or the loss of FBL and UBF genes that play a role in the extinction of nucleolus activity.[33,48,49] In addition, we showed that ribosome biogenesis arrest coincides with the delocalization of nucleolar DDX21, suggesting that the RNA Pol I complex could be destabilized.[34] DDX21 eviction is concomitant to rDNA damage in genetic models mimicking congenital ribosomopathies such as Treacher-Collins syndrome, which is caused by mutations in RNA Pol I complex subunits, Diamond-Blackfan anemia, or Schwachman-Diamond syndrome, or after treatment with high concentrations of CX-5461.[50,51] Whether DDX21 eviction in maturing erythroblasts means the loss of RNA Pol I complex recruitment or a more complex chromatin structural remodeling similar to rDNA damage remains to be defined.

p53 has been shown to inhibit RNA Pol I transcription by preventing the RNA Pol I complex assembly on rDNA promoter.[52] The use of a direct activator of p53 (NSC146109) induced DDX21 nucleolar extrusion and the arrest of eU incorporation into rRNA, showing that p53 overactivation induces a ribosomal stress.[50] Also, ribosome biogenesis is overactivated in cancer cells, notably by a loss of function of RNA Pol I repressors, such as p53,[30,52] which suggests that p53 activation could amplify the inhibition of rDNA transcription and restrain ribosome biogenesis and subsequently cell proliferation.

In summary, our findings regarding the role of ribosome biogenesis in erythroid development are supported by the recognition of erythroid defects in ribosomopathies. The timing of ribosome biogenesis extinction and p53 activation is crucial for erythroid differentiation. In ribosomopathies in which ribosome availability is altered by unbalanced production, the threshold of ribosome biogenesis downregulation could be prematurely reached, thus preventing a normal expansion of erythroid progenitors.

Acknowledgments

The authors thank O. Kosmider (Institut Cochin, Paris, France), L. Da Costa (Hôpital R Debré, Paris, France), and M.-F. O'Donohue (Laboratoire de Biologie Moléculaire Eucaryote, Centre de Biologie Intégrative, Université de Toulouse, Toulouse, France) for helpful discussions; K. Labroquère and M. Andrieu (Institut Cochin CYBIO Facility), T. Guilbert and P. Bourdoncle (Institut Cochin Photonic Imaging Facility [IMAG'IC]), J. M. Massé and A. Schmitt (Electron Microscopy Facility), and A. Baudin-Baillieu, S. Hermann-Le Denmat, P. Facek, E. Quiot, and A. Pajot for technical assistance; and N. Fernandez Vñez and B. Loriaud (Transcriptomics and Genomics of Marseille-Luminy [TGML], Marseille, France) for excellent support with the Illumina high-throughput sequencing performed on the TGML platform.

This work was supported by INSERM–Institut Thématique Multi-Organismes (ITMO)–Immunologie Hématologie Pneumologie grant IHP-2012 and by National Institutes of Health, National Institute of Diabetes and Digestive and Kidney Diseases grant DK32094. S.L.G. received a grant from the LabEx GR-Ex (reference ANR-11-LABX-0051). The Labex GR-Ex is funded by the program "Investissements d'Avenir" of the French National Research Agency (reference ANR-18-IDEX-0001). I.B. received a grant from ArDoc from the Région Ile de France. C.F. was supported by a fellowship from the Fondation de France and from Agence Nationale pour la Recherche (ANR Blanc 2013). A.R. was supported by a fellowship from the Fondation ARC pour la Recherche contre le Cancer. E.S., C.A.-S., and M.S. were supported by the Fondation pour la Recherche Médicale (Equipe FRM DEQ20180339221), and the Labex EpiGenMed (Investissements d'Avenir Program, reference ANR-10-LABX-12-01). The TGML platform is supported by grants from INSERM, Groupement d'Intérêt Scientifique-Infrastructures en Biologie Santé et Agronomie (GIS-IBiSA), Aix-Marseille Université, and ANR-10-INBS (Institute of Biological Sciences)-0009-10. F. Dumont (Genomics Facility) was supported by the Site de Recherche Intégrée sur le Cancer (SIRIC) CARPEM.

Authorship

Contribution: F.M., P.-E.G., C.F., P.M., and M.F. designed the study; S.L.G., I.B., C.F., A.R., B.G., I.H., A.H., D.d.A., N.M.-L., C.A.-S., E.-F.G.,

S.D., S.K., M.L., S.G., and R.-A.P. performed the experiments; S.L.G., I.B., C.F., A.R., B.G., F.M., P.-E.G., N.M.-L., F.V., S.D., S.K., E.C.-B., F.G,. P.M., M.S., N.M., E.S., N.T., N.M.-L., O.H., J.-J.D., and R.-A.P. analyzed the data; M.F. wrote the manuscript; and all authors critically reviewed the manuscript.

Conflict-of-interest disclosure: The authors declare no competing financial interests.

ORCID profiles: A.R., 0000-0002-7368-2247; I.H., 0000-0002-4428-3079; M.L., 0000-0002-4049-3976; F.G., 0000-0003-1484-4696; S.G., 0000-0002-1817-2236; R.-A.P., 0000-0001-9964-7864; N.M., 0000-0003-2271-5296; P.-E.G., 0000-0003-0830-7341; E.S., 0000-0003-0521-7463; M.F., 0000-0002-5492-6349.

Correspondence: Michaela Fontenay, Institut Cochin, 22 rue Méchain, F-75014 Paris, France; e-mail: michaela.fontenay@inserm.fr.

Footnotes

Submitted 24 September 2019; accepted 3 August 2020; prepublished online on *Blood* First Edition 20 August 2020. DOI 10.1182/blood.2019003439.

*S.L.G. and I.B. are joint first authors.

†C.F. and A.R. are joint second authors.

The data reported in this article have been deposited in the Gene Expression Omnibus database (accession number GSE157210).

The online version of this article contains a data supplement.

The publication costs of this article were defrayed in part by page charge payment. Therefore, and solely to indicate this fact, this article is hereby marked "advertisement" in accordance with 18 USC section 1734.

REFERENCES

1. Dolznig H, Grebien F, Sauer T, Beug H, Müllner EW. Evidence for a size-sensing mechanism in animal cells. *Nat Cell Biol*. 2004; 6(9):899-905.

2. Lodish H, Flygare J, Chou S. From stem cell to erythroblast: regulation of red cell production at multiple levels by multiple hormones. *IUBMB Life*. 2010;62(7):492-496.

3. Hu J, Liu J, Xue F, et al. Isolation and functional characterization of human erythroblasts at distinct stages: implications for understanding of normal and disordered erythropoiesis in vivo. *Blood*. 2013;121(16):3246-3253.

4. Hattangadi SM, Wong P, Zhang L, Flygare J, Lodish HF. From stem cell to red cell: regulation of erythropoiesis at multiple levels by multiple proteins, RNAs, and chromatin modifications. *Blood*. 2011;118(24): 6258-6268.

5. Kerenyi MA, Orkin SH. Networking erythropoiesis. *J Exp Med*. 2010;207(12):2537-2541.

6. An X, Schulz VP, Li J, et al. Global transcriptome analyses of human and murine terminal erythroid differentiation. *Blood*. 2014;123(22):3466-3477.

7. Welch JJ, Watts JA, Vakoc CR, et al. Global regulation of erythroid gene expression by transcription factor GATA-1. *Blood*. 2004; 104(10):3136-3147. /blood-2004-04-1603

8. Munugalavadla V, Dore LC, Tan BL, et al. Repression of c-kit and its downstream substrates by GATA-1 inhibits cell proliferation during erythroid maturation. *Mol Cell Biol*. 2005;25(15):6747-6759.

9. Lodish HF. Model for the regulation of mRNA translation applied to haemoglobin synthesis. *Nature*. 1974;251(5474):385-388.

10. Fromont-Racine M, Senger B, Saveanu C, Fasiolo F. Ribosome assembly in eukaryotes. *Gene*. 2003;313:17-42.

11. Henras AK, Plisson-Chastang C, O'Donohue MF, Chakraborty A, Gleizes PE. An overview of pre-ribosomal RNA processing in eukaryotes. *Wiley Interdiscip Rev RNA*. 2015;6(2):225-242.

12. Draptchinskaia N, Gustavsson P, Andersson B, et al. The gene encoding ribosomal protein S19 is mutated in Diamond-Blackfan anaemia. *Nat Genet*. 1999;21(2):169-175.

13. Gazda HT, Sheen MR, Vlachos A, et al. Ribosomal protein L5 and L11 mutations are associated with cleft palate and abnormal thumbs in Diamond-Blackfan anemia patients. *Am J Hum Genet*. 2008;83(6):769-780.

14. Ebert BL, Pretz J, Bosco J, et al. Identification of RPS14 as a 5q− syndrome gene by RNA interference screen. *Nature*. 2008;451(7176): 335-339. Available from: https://doi.org/10.1038/nature06494

15. Khajuria RK, Munschauer M, Ulirsch JC, et al. Ribosome Levels Selectively Regulate Translation and Lineage Commitment in Human Hematopoiesis. *Cell*. 2018;173(1):90-103.e19.

16. Ludwig LS, Gazda HT, Eng JC, et al. Altered translation of GATA1 in Diamond-Blackfan anemia. *Nat Med*. 2014;20(7):748-753.

17. Boussaid I, Le Goff S, Floquet C, et al. Integrated analyses of translatome and proteome identify the rules of translation selectivity in RPS14-deficient cells [published online ahead of print 23 April 2020]. *Haematologica*. doi:10.3324/haematol.2019.239970.

18. Dutt S, Narla A, Lin K, et al. Haploinsufficiency for ribosomal protein genes causes selective activation of p53 in human erythroid progenitor cells. *Blood*. 2011;117(9):2567-2576.

19. Moniz H, Gastou M, Leblanc T, et al; DBA Group of Société d'Hématologie et d'Immunologie Pédiatrique-SHIP. Primary hematopoietic cells from DBA patients with mutations in RPL11 and RPS19 genes exhibit distinct erythroid phenotype in vitro. *Cell Death Dis*. 2012;3(7):e356.

20. Gautier EF, Ducamp S, Leduc M, et al. Comprehensive Proteomic Analysis of Human Erythropoiesis. *Cell Rep*. 2016;16(5): 1470-1484.

21. Gautier EF, Leduc M, Ladli M, et al. Comprehensive proteomic analysis of murine terminal erythroid differentiation. *Blood Adv*. 2020;4(7):1464-1477.

22. O'Donohue M-F, Choesmel V, Faubladier M, Fichant G, Gleizes P-E. Functional dichotomy of ribosomal proteins during the synthesis of mammalian 40S ribosomal subunits. *J Cell Biol*. 2010;190(5):853-866.

23. Cox J, Matic I, Hilger M, et al. A practical guide to the MaxQuant computational platform for SILAC-based quantitative proteomics. *Nat Protoc*. 2009;4(5):698-705.

24. Wiśniewski JR, Hein MY, Cox J, Mann M. A "proteomic ruler" for protein copy number and concentration estimation without spike-in standards. *Mol Cell Proteomics*. 2014;13(12): 3497-3506.

25. Ali A, Bluteau O, Messaoudi K, et al. Thrombocytopenia induced by the histone deacetylase inhibitor abexinostat involves p53-dependent and -independent mechanisms. *Cell Death Dis*. 2013;4(7):e738.

26. Jacks T, Remington L, Williams BO, et al. Tumor spectrum analysis in p53-mutant mice. *Curr Biol*. 1994;4(1):1-7.

27. Stadhouders R, Aktuna S, Thongjuea S, et al. HBS1L-MYB intergenic variants modulate fetal hemoglobin via long-range MYB enhancers. *J Clin Invest*. 2014;124(4):1699-1710.

28. Stadhouders R, Cico A, Stephen T, et al. Control of developmentally primed erythroid genes by combinatorial co-repressor actions. *Nat Commun*. 2015;6(1):8893.

29. Reschke M, Clohessy JG, Seitzer N, et al. Characterization and analysis of the composition and dynamics of the mammalian riboproteome. *Cell Rep*. 2013;4(6):1276-1287.

30. Bywater MJ, Poortinga G, Sanij E, et al. Inhibition of RNA polymerase I as a therapeutic strategy to promote cancer-specific activation of p53. *Cancer Cell*. 2012;22(1): 51-65.

31. Xu J, Shao Z, Glass K, et al. Combinatorial assembly of developmental stage-specific enhancers controls gene expression programs during human erythropoiesis. *Dev Cell*. 2012; 23(4):796-811.

32. Huang J, Liu X, Li D, et al. Dynamic control of enhancer repertoires drives lineage and stage-specific transcription during hematopoiesis. *Dev Cell*. 2016;36(1):9-23.

33. Hernandez-Verdun D. The nucleolus: a model for the organization of nuclear functions. *Histochem Cell Biol*. 2006;126(2):135-148.

34. Calo E, Flynn RA, Martin L, Spitale RC, Chang HY, Wysocka J. RNA helicase DDX21 coordinates transcription and ribosomal RNA processing. *Nature*. 2015;518(7538):249-253.

35. Jossé R, Martin SE, Guha R, et al. ATR inhibitors VE-821 and VX-970 sensitize cancer

cells to topoisomerase I inhibitors by disabling DNA replication initiation and fork elongation responses. *Cancer Res*. 2014;74(23):6968-6979.

36. Fumagalli S, Di Cara A, Neb-Gulati A, et al. Absence of nucleolar disruption after impairment of 40S ribosome biogenesis reveals an rpL11-translation-dependent mechanism of p53 induction. *Nat Cell Biol*. 2009;11(4):501-508.

37. Donati G, Peddigari S, Mercer CA, Thomas G. 5S ribosomal RNA is an essential component of a nascent ribosomal precursor complex that regulates the Hdm2-p53 checkpoint. *Cell Rep*. 2013;4(1):87-98. /j.celrep.2013.05.045

38. Jaako P, Debnath S, Olsson K, et al. Disruption of the 5S RNP-Mdm2 interaction significantly improves the erythroid defect in a mouse model for Diamond-Blackfan anemia. *Leukemia*. 2015;29(11):2221-2229.

39. Danilova N, Sakamoto KM, Lin S. Ribosomal protein S19 deficiency in zebrafish leads to developmental abnormalities and defective erythropoiesis through activation of p53 protein family. *Blood*. 2008;112(13):5228-5237.

40. Barlow JL, Drynan LF, Hewett DR, et al. A p53-dependent mechanism underlies macrocytic anemia in a mouse model of human 5q− syndrome. *Nat Med*. 2010;16(1):59-66.

41. Bhat KP, Itahana K, Jin A, Zhang Y. Essential role of ribosomal protein L11 in mediating growth inhibition-induced p53 activation. *EMBO J*. 2004;23(12):2402-2412.

42. Ganguli G, Back J, Sengupta S, Wasylyk B. The p53 tumour suppressor inhibits glucocorticoid-induced proliferation of erythroid progenitors. *EMBO Rep*. 2002;3(6):569-574.

43. Zermati Y, Garrido C, Amsellem S, et al. Caspase activation is required for terminal erythroid differentiation. *J Exp Med*. 2001;193(2):247-254.

44. Brady CA, Jiang D, Mello SS, et al. Distinct p53 transcriptional programs dictate acute DNA-damage responses and tumor suppression. *Cell*. 2011;145(4):571-583.

45. Papetti M, Wontakal SN, Stopka T, Skoultchi AI. GATA-1 directly regulates p21 gene expression during erythroid differentiation. *Cell Cycle*. 2010;9(10):1972-1980.

46. Hu W, Yuan B, Lodish HF. Cpeb4-mediated translational regulatory circuitry controls terminal erythroid differentiation. *Dev Cell*. 2014;30(6):660-672.

47. Trainor CD, Mas C, Archambault P, Di Lello P, Omichinski JG. GATA-1 associates with and inhibits p53. *Blood*. 2009;114(1):165-173.

48. Barna M, Pusic A, Zollo O, et al. Suppression of Myc oncogenic activity by ribosomal protein haploinsufficiency. *Nature*. 2008;456(7224):971-975.

49. Juban G, Giraud G, Guyot B, et al. Spi-1 and Fli-1 directly activate common target genes involved in ribosome biogenesis in Friend erythroleukemic cells. *Mol Cell Biol*. 2009;29(10):2852-2864.

50. Calo E, Gu B, Bowen ME, et al. Tissue-selective effects of nucleolar stress and rDNA damage in developmental disorders. *Nature*. 2018;554(7690):112-117.

51. Sanij E, Hannan KM, Xuan J, et al. CX-5461 activates the DNA damage response and demonstrates therapeutic efficacy in high-grade serous ovarian cancer. *Nat Commun*. 2020;11(1):2641.

52. Zhai W, Comai L. Repression of RNA polymerase I transcription by the tumor suppressor p53. *Mol Cell Biol*. 2000;20(16):5930-5938.